ORIGINAL PAPER

Kinematic tests on a docking mechanism for microsatellites

Luca Lion[1] · Alex Caon[1] · Lorenzo Olivieri[1] · Francesco Branz[2] · Alessandro Francesconi[2]

Abstract
DOCKS is a smart docking system developed within the framework of the Space Rider Observer Cube mission (SROC) but suitable for use in more general scenarios. This paper presents the mechanical design of the system and the kinematic tests performed on it. The system merges a classical probe drogue configuration with a gripper-like design, to manage the connection between the parts, and it is equipped with a suite of sensors to estimate the relative pose of the target. The system is also equipped with a dedicated computer, making it a smart standalone system. A series of kinematic tests have been conducted to validate the capability of the system to passively manage misalignment during the docking manoeuvre. The final tests are presented to assess the maximum load that the system could handle, even when inactive.

Keywords Docking mechanism · Smart system · Microsatellites · CubeSat

Abbeviations

EM	Electromagnet
FDM	Fused Deposition Modeling
GNC	Guidance, Navigation and Control
LED	Light-Emitting Diode
MPCD	Multi-Purpose CubeSat Dispenser
NavCam	Navigation Camera
SLA	StereoLitogrAphy
SR	Space Rider
SROC	Space Rider Observer Cube
ToF	Time of Flight Sensors

✉ Luca Lion
   luca.lion.1@phd.unipd.it

   Alex Caon
   alex.caon@unipd.it

   Lorenzo Olivieri
   lorenzo.olivieri@unipd.it

   Francesco Branz
   francesco.branz@unipd.it

   Alessandro Francesconi
   alessandro.francesconi@unipd.it

[1] Centre of Studies and Activities for Space (CISAS) "Giuseppe Colombo", University of Padova, via Venezia, 15, Padova 35131, Italy

[2] Department of Industrial Engineering, University of Padova, via Venezia, 1, Padova 35131, Italy

1 Introduction

The Space Rider Observer Cube (SROC) mission is designed to be a payload on the ESA Space Rider (SR) project. The main objective of the mission is to demonstrate the critical capabilities and technologies required to execute a rendezvous and docking mission in a safety-sensitive context. The space system is composed by a nanosatellite (12U CubeSat) and a deployment/retrieval mechanism mounted inside the payload bay of SR. During the mission, SROC will be released by SR, will perform inspection manoeuvres on SR and, at the end of the mission, it will dock back inside the bay of SR, before re-entering Earth. The mission will prove innovative key technologies in the area of proximity operations including: Guidance, Navigation and Control (GNC) system (both software and hardware) and systems for docking, deployment and retrieval. SROC will fly in formation with SR and demonstrate the aforementioned technologies that could be then transferred to other targets and missions ([1]).

The SROC mission operations can be divided into five main phases:

1. Launch and early operations. SROC will be launched inside the bay of SR and release into space through a dedicated mechanism, the Multi-Purpose CubeSat Dispenser (MPCD).

2. Commissioning and performance verification phase. The critical capabilities for proximity operation will be verified and SROC will be put on a safe trajectory.
3. Proximity operations. SROC will perform close observation cycles of SR starting from 300km away to a distance below 5km;
4. Docking and retrieval. SROC will perform the final approach to SR, will dock to MPCD and finally will be retrieved inside the payload bay of SR;
5. End of mission. SROC will re-entry back to Earth together with SR. After landing SROC and MPCD will be uninstalled from SR and checked out.

In this paper, the docking mechanism developed for the mission is presented. The interest in developing technologies for missions aimed at In Orbit Servicing and In Orbit Assembly is increasing with the enthusiasm towards small satellites, in particular nanosatellites (<10kg) and microsatellites (<100kg). During the years, multiple designs have been presented. The probe–drogue design is one of the simplest and has been largely used in the past ([2–5]). Other solutions have been presented and implemented over the years from magnetic to semi-androgynous ([6–11]). In addition to the one specifically designed for the space segment, a design based on the gripper used in the industrial environment has been considered during the development of the system ([12]).

The system is not strictly designed to be used only on the SROC mission, but also represents a viable solution for the small satellites market in general.

The system design proposed in this paper comes from a trade-off between multiple design solutions. Various design solution both from literature and internally designed are considered in the trade-off. From each solutions, the key characteristics are extrapolated and analyzed. The system described in this paper proposes an innovative docking mechanism, which merges together the benefits of different state of the art alternatives with little to none compromises.

The design proposed here is based on a probe–drogue configuration aided by a gripper-style system to ensure the hard docking. The system requires that the target is prepared, but not necessarily cooperative. In fact, a cooperative target is capable of controlling its own attitude and communicating with the chaser. A prepared one does not have this capabilities and it is only required to have mounted on itself the docking counterpart. In addition to the mechanism, a suite of sensors is added to manage ultra-close proximity operations.

To validate the system a series of kinematic tests have been conducted to characterize the misalignment tolerances.

The remainder of the paper is organised as follows: Sect. 2 describes the concept behind the system and the design drivers; Sect. 3 briefly presents the sensor suite mounted on the system; Sect. 4 illustrates the requirements and the description of all the components of the system; Sect. 5 shows the budgets of the system in terms of mass, power, volume and data; Sect. 6 discusses the test setup, procedure and results for the misalignment characterisation; Sect. 7 presents the load test methodology and results; Sect. 8 presents the conclusions.

2 DOCKS design objectives

The concept at the base of the project is to create a standalone system capable of managing the docking phase, from ultra-close proximity (< 1m) until safe connection.

Figure 1 shows a schematic overview of the system that highlights the interfaces between the system and the bus (SROC and SR). DOCKS–A is connected to SROC via mechanical, power, and data interfaces. DOCKS–B, does not require data support and is connected to MPCD only through mechanical and power interfaces.

The system is composed of three main elements: mechanical, sensors, and control logic. The control logic is managed by a dedicated computer. Due to the presence of a dedicated logic, the system is referred as *smart*. All these components are located on one single part (DOCKS–A), considered to be on the chaser satellite.

The target is then equipped with a completely passive interface (DOCKS–B). This configuration allows the system to be more ductile in the context of future different missions. In fact, the target does not need to be cooperative, but only prepared.
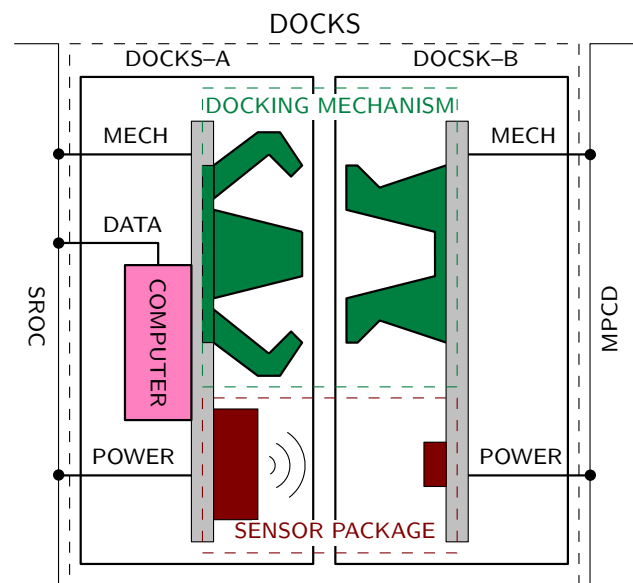

Fig. 1 Schematic representation of DOCKS and its interfaces with SROC and MPCD
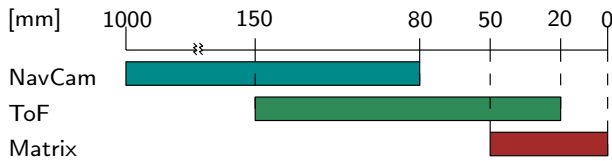
Fig. 2 Representation of the ranges covered by each of the three sensors included in DOCKS

The sensor suite has the purpose of retrieving the relative pose of the target in the last metre. The last element of the system is the mechanism (Sect. 4), which enables the docking by ensuring the alignment and connection between the two parts.

3 Sensor suite

The DOCKS relative navigation sensor suite is composed of:

1. Navigation Camera (NavCam);
2. Four Time of Flight sensors (ToF);
3. Matrix sensor;

Each of the three sensors covers different ranges and different measurements (Fig. 2). The sensor suite is composed in this way to offer measures from 1m relative distance up to contacts. The measurement interval of the sensors overlaps during the transition between one and the other. The NavCam (Raspberry Pi Camera Module V2.1) is employed between 1m and 80mm. This sensor can retrieve the complete relative pose of the target ([13]). To do so, two patterns of fiducial LED (light–emitting diode) markers are used to cover different distances (RS 132-9151). The ToF sensors (Adafruit VL6180X) are used to retrieve the relative distance between the chaser and the target and the relative rotations of the target around the x and y axes ([14]), the reference frame is shown in Fig. 3. The matrix sensor consists of two parts: a 5×5 array of phototransistors (OSRAM SFH 309) and an IR LED (infrared light–emitting diode, OKingbright L-7104F3C). Depending on the distance, the IR LED activates a different number of phototransistors. From the position and number of active phototransistors, it is possible to compute the position of the target along the x and y axes ([15]).

On DOCKS–A are also present three fork sensors. These are not considered part of the sensor suite since their purpose is not to retrieve the pose of the target, but only to provide the activation signal to the claws and act as acknowledgment for the the soft-docking. These sensors are described in Sect. 4.2.

(a) Laboratory prototype of the docking system.
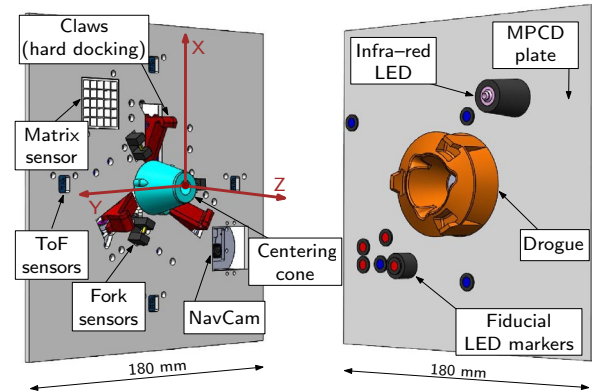
(b) 3D CAD model.

Fig. 3 Docking system: on the left DOCKS–A and on the right DOCKS-B

4 Docking mechanism

The core of DOCKS is the docking mechanism, whose main function is to provide a rigid connection between the target and the chaser. Additionally, the mechanism must be able to manage some misalignment to compensate for limitations in the GNC subsystem performance and provide a soft docking capability by managing contact forces and potential rebounces. The requirements for the system and the design choices will be presented in the following sections.

4.1 Requirements

The majority of requirements derived from the SROC mission architecture and design. The requirements derived for the mechanical system are the following:

R1 The system shall provide a rigid connection (hard docking) between the target and the chaser.
R2 The system shall implement multiple locking mechanisms that can be actuated independently and provide redundancy.

R3 The mechanical system shall fit in a compact volume of 0.5 Unit of CubeSat.

R4 The system shall not contain any sliding mechanism, to reduce wear and the risk of jamming.

R5 The system shall have an axial–symmetric design, to allow easier integration in the bus, and shall not exceed a circular planar envelope of 100mm in diameter.

R6 The system shall provide passive self-centering capabilities and shall be able to tolerate a lateral misalignment of ± 8mm (along x and y, see Fig. 3), an angular misalignment of ± 6deg around z and of ± 3deg around x and y.

R7 The system shall provide magnetic soft-docking capabilities and grant a holding force of at least 5N.

4.2 Mechanical design

The proposed design is a combination of the probe-drogue design and a gripper-like mechanism concept. Figure 3 shows the two parts of the docking system, DOCKS–A on the left and DOCKS–B on the right. The docking reference frame is also shown: the z axis pointing from DOCKS–A towards DOCKS–B, the x axis is vertical in the reference frame of the laboratory and the y axis to complete the left-handed tern. The relative rotations are defined as follow: roll around the z axis, yaw around the x axis and pitch around the y axis.

The main components of the mechanism hosted on DOCKS–A are the centering cone, the claws, the fork sensors and the electromagnet. The centering cone on DOCKS–A provides the self-alignment for DOCKS and would represent the probe in an equivalent probe/drogue baseline configuration. The dimensions of the cone are shown in Fig. 4. The passive drogue on DOCKS–B (Fig. 3 right) acts as a counterpart for the centering cone and the claws.
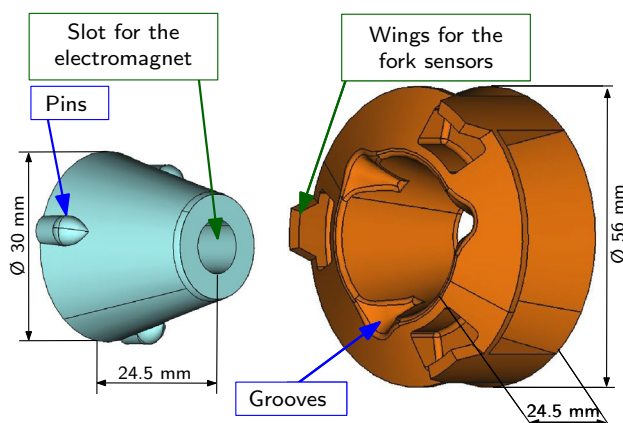
The conic shape of the probe eases the in-plane, yaw, and pitch angular alignment. The self-alignment in the roll is managed by the pins and the grooves. The design of the grooves allows the centering cone to be guided in the correct position and to lock the rotation when the insertion is complete. The self-alignment is achieved thanks to the centering cone and the drogue geometry. Three protruding wings are intended to trigger the fork sensors in DOCKS–A, while the external sloped perimeter is necessary to offer a grasping surface for the claws.

The soft-docking is defined as the establishment of a non-rigid connection between the two parts. The solution presented in this paper revolves around the use of magnetic force. In fact, the centering cone hosts the electromagnet (EM) that when activated and in contact with the counter pats generates the required holding force (see Fig. 4). The purpose of the soft-docking is to reduce the risk of bouncing when the probe is entering the drogue and to allow a first temporary connection before the claws are activated. For this design, a commercially available 12V electromagnet has been selected to allow a fast prototyping approach (Mecalectro–Safety holding electromagnet 5.11.05). The EM is activated at the beginning of the docking procedure and shuts off after the hard docking is achieved.

To obtain the rigid connection between DOCKS–A and DOCKS–B, three claws are installed around the centering cone, angularly spaced by 120deg. The hard docking is established when all the claws are closed around the rim of the drogue.

Each claw is connected to a four-bar linkage actuated by a servo motor. This choice allows to avoid sliding contacts that can stall the mechanism and linear actuators, since their volume is higher in comparison with rotational motors.

The four-bar linkage (Fig. 5) has a total angular movement, α, of 57deg. This value is set to allow the use of frictionless pivot bearings, in particular flexural pivot ([16]), the ones considered for the design are Free-Flex Pivots 800 series.

The laboratory prototype is equipped with commercial motors (Kitronic Mini 180 Degree Servo).
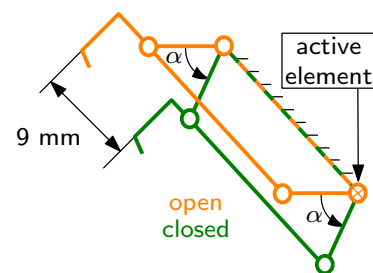

Fig. 4 Left: centering cone, at the base the pin that forces the roll alignment. Right: the drogue, at the top the three wings to activate the fork sensors, and the grooves that accommodate the pins

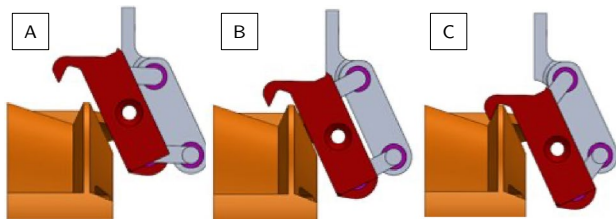**Fig. 5** Scheme of the claw four-bar linkage mechanism

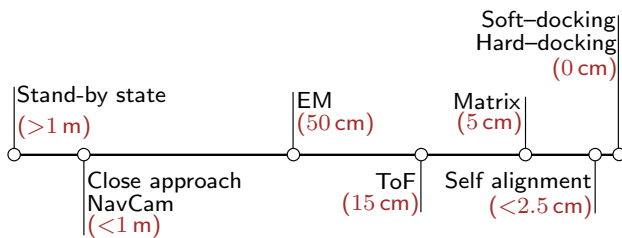**Fig. 6** Actuation sequence of a closing claw

Fig. 7 Schematic overview of the docking sequence of operations in relation with relative distance

The design of the claws and its counterpart on the drogue allows to manage a misalignment along the z axis of approximately 3mm. The closing sequence of the claw is visible in Fig. 6, where in (A) the claw is completely open and in (C) it is fully closed. In Step (B), the claw is only partially closed, but it is already able to grasp the drogue, nullifying the residual misalignment along z. This design allows to maintain a rigid connection between DOCKS–A and DOCKS–B even in case of failure of one of the claws, providing redundancy as requested by the requirements.

Three fork sensors acknowledge the soft-docking if they are continuously activated for at least 2s, to reduce the risk of false signal caused by possible bounces during the manoeuvre. The fork sensors also provide the activation signal for the closing procedure of the claws. Only two fork sensors are necessary to provide the acknowledgment of the soft docking, but the choice of having three was made to guarantee redundancy.

4.3 Docking procedure

DOCKS operates during the final phase of the approach, when SROC is getting close, under 1m, to MPCD on Space Rider, and during the retrieval phase after docking. DOCKS is activated at the last waiting point in the approach trajectory, around 100m from SR. A preliminary sequence of operations of DOCKS is as follows (Fig. 7):

1. *Stand-by state* (>1 m). DOCKS is powered on; the local computer communicates with SROC for telemetry; the sensors are active but out of range; the LED fiducial markers and beacon are active; the actuators and the electromagnet are idle.

2. *Close approach* (<1 m). As SROC approaches MPCD, the relative distance is within the operating range of the navigation camera.

   — *Pose estimation*. DOCKS provides SROC with pose estimates and will continue doing so until the docking is completed.

   ▌ *Navcam navigation* $(100 \div 8)$cm. The local PC collects images of the LED pattens from the camera system, performs image analysis and estimates the relative pose of DOCKS–B with respect to DOCKS–A;
   ▌ *Ultra close approach – ToF* $(15 \div 2$cm$)$. As the relative distance reduces below 0.15m, the set of ToF sensors is in range. ToF sensors provide measurements of the relative distance and two orientations (yaw and pitch);
   ▌ *Ultra close approach – matrix* $(5 \div 0$cm$)$. As the relative distance decreases below 0.05 m, the matrix sensor retrieves the relative the position along the x and y axes.
   ▌ *Ultra close approach – matrix and ToF* $(15 \div 0)$cm. The data from the NavCam, the ToF and the matrix are used to extrapolate the pose of the target thanks to a dedicated estimation algorithm;

   — *EM activation* $(< 0.5m)$. When the relative distance is less than 0.5m, the electromagnet is activated.
   — *Self alignment* $(< 2.5cm)$. The relative distance is in the order of a few centimetres, and the contact between the probe and the drogue allows DOCKS–A to self–align with DOCKS–B.

3. *Contact*

   Soft docking. As soon as the probe is fully inserted in the drogue, the electromagnet enters in contact with the ferromagnetic plate and generates the soft-docking holding force.
   — *Fork sensor activation* $(< 3mm)$. DOCKS–A and DOCKS–B are in full contact, and acknowledgement signals are provided by the fork sensors.
   Hard docking. The claws are actuated following the closure command provided by DOCKS computer; the claws lock the connection.
   — *Retrieval*. A docking signal is provided to SROC; MPCD begins the retrieval procedure; the navigation sensors are switched off; the electromagnet is

Table 1 Volume envelope of DOCKS–A and DOCKS–B

	Internal protrusion ($-z$) [mm]	External protrusion ($+z$) [mm]	Circular envelope [mm]
DOCKS-A	25	24.5	83
DOCKS-B	0	24.5	56

Table 2 Mass budget for DOCKS–A and DOCKS–B

Component	Mass [g]
DOCKS–A	
3× claw	50
Centering cone	13
Electromagnet	35
3× motors and structure	40
Sensors	61
Total	199
Total +30% margin	272
DOCKS–B	
Drogue	105
Sensors	30
Total	135
Total +30% margin	176

switched off; the hard-docking actuators are kept powered until the retrieval of SROC is completed by MPCD.

4. *Re–entry*. SROC is safely stored inside the Multi–Purpose Cargo Bay of Space Rider and ready to re-enter back to Earth.

5 Budgets

A first iteration on the volume, mass, power, and data budgets has been conducted based on the characteristics of the DOCKS laboratory prototype. These budgets are only partially representative of those of a future flight model. To account for the lack of confidence in these estimates, margins of 30% for the mass and for the power are considered.

Volume. Table 1 summarises the volume envelope of DOCKS–A and DOCKS–B. On DOCKS-A, the mechanical system occupies less then 0.4U to witch 0.25U (approximately) must be added for the dedicated computer. On DOCKS–B, the volume occupied by the drogue is less than 0.1U. In these estimations, the sensors are not taken into account, because they can be positioned where needed to avoid getting in the way of other components.

Mass. The laboratory prototype of DOCKS is manufactured mainly in polymers and its mass is not representative. The estimate of the mass budget considers all components as made of aluminium (see Table 2).

Power. Table 3 presents a preliminary power budget for DOCKS–A, which is the most power-demanding part of DOCKS. DOCKS–A absorbs different levels of power depending on which sensors and actuators are turned on during the various operation phases. The presented estimation of power consumption is based on the performance of the laboratory prototype of DOCKS: the considered actuators are micro-servo motors, while the electronic boards are one Raspberry Pi Model 3+ and one Arduino UNO Rev3. The estimation is only loosely representative of a flight model of DOCKS, for this reason, a 20% margin is considered.

On DOCKS–B, no power is required for the mechanism to work. In fact, the drogue is a completely passive component. The only components that draw power are the LEDs (visible and IR) used by the navigation sensor package. An estimate of the total power consumption of these components is 2W. To highlight when the components are active or not, the sequence has been divided into four phases: (A) close approach, when the chaser is 1m further away from the target, (B) ultra close approach, when the target is closer than 1m from the target, (C) mating, the target and the chaser are in contact and (D) docking, the docking manoeuvre takes place.

Data. DOCKS–A and its computer have two data streams: one from each navigation sensor to the computer of DOCKS-A and the other from this computer to the main computer of SROC. Taking into account a sampling time of 0.1s, the preliminary estimates of the data rate for both streams are (Fig. 8):

140MB/s from the sensors to the local computer.
2560B/s from DOCKS–A to SROC, including a 100% margin.

6 Test management and results

The objective of these tests is to evaluate the performance of the docking system in terms of misalignment tolerance with respect to the extrapolated data from the CAD model. To do so, a series of tests have been carried out involving the use of the robotic arm and the motion capture system described in Sect. 6.1.

The tests carried out on DOCKS are purely kinematic. In this case, there is no representation of the orbital environment or of the other components of the satellites. The system is tested as standalone. The forces exchanged between the parts are not considered.

Table 3 The upper table represents the power budget of DOCKS–A, while the other table shows the power consumption of DOCKS–B. In both tables, the first row identifies an operation timeline divided into phases: A close approach 1 m; B ultra close approach 1 m; C mating; D docking

DOCKS–A	Power [W]	A	B	C	D
Electromagnet	1.50				
3× Fork sensors	0.75				
3× Motors idle	1.30				
3× Motors active	7.90				
Sub–Total		1.30	2.05	10.15	7.90
Sub–Total +30% margin		1.69	2.66	13.19	10.27
NavCam	2.55				
3× ToF	0.01				
Matrix sensor	0.06				
Sub–Total		0	2.62	2.62	0
Sub–Total +30% margin		0	3.42	3.42	0
Total		1.30	4.67	12.77	7.90
Total +30% margin		1.69	6.07	16.60	10.27

DOCKS–B	Power [W]	A	B	C	D
LED (NavCam)	1.80				
IR LED (matrix)	0.20				
Total		2.00	2.00	2.00	2.00
Total +30% margin		2.60	2.60	2.60	2.60

6.1 Test setup

The facility equipment used during the tests is composed by: a custom 6 DoF robotic arm designed to act as a moving
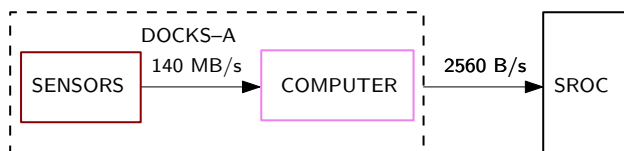

Fig. 8 Schematic representation of the data transfer from the sensor package to the computer and from the computer to the SROC bus

system to simulate docking/capture ([17]) and a 4–camera motion capture system (OptiTrack Prime^x 13 with an accuracy of 0.2mm) that is focused on the workspace of the robotic arm. The motion capture system acts as a ground truth and will provide a relative reference measure between the two parts under test. The facility is visible in Fig. 9.

During the test campaign, DOCKS–A is rigidly connected to the end–effector of the robotic arm. The mounting configuration for DOCKS–B varies depending on the test performed. In each configuration, 5 DoFs are locked and only one is left free to move. To test lateral misalignment, DOCKS–B is mounted on a linear rail free to move along the y axis (see Fig. 10a). During the roll self–alignment test, DOCKS–B is connected to the supporting structure
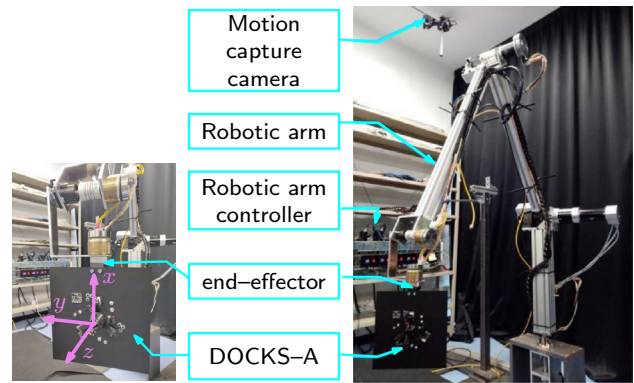

Fig. 9 The facility employed for the test performed on DOCKS. It is composed by a 6 DoF robotic arm (right) equipped with a spherical end–effector on which DOCKS–A is mounted (left)

through a ball bearing that allows rotation along the z axis (see Fig. 10b). For the configuration that involves yaw rotation, DOCKS–B is connected to an external structure along the x axis through two bearings (see Fig. 10c). The axis of rotation is set to be in the middle of the plate. Thanks to the fact that the system is axially symmetric, the results obtained for the rotation around the x axis (yaw) can be considered valid also for the rotation around the y axis (pitch). The last test performed is along the z axis. In this case, DOCKS–A is rigidly connected to the structure, while DOCKS–B is fixed on a linear rail and left free to move along the z axis (see Fig. 10d).

Since the exact position of the drogue with respect to the MPCD plate has not been defined (see Fig. 3), the tests for the determination of the tolerance for yaw misalignment have been repeated in three configurations visible in Fig. 11:

A   The base of the drogue is coplanar with the MPCD plate.
B   The base of the drogue is 15mm below the MPCD plate.
C   The top of the drogue is coplanar with the MPCD plate.

The tests in these three configurations provide an assessment of the influence of the position of the plate on the tolerance to yaw misalignment.

The DOCKS prototype model used during these tests is realised using mainly 3D printed parts. The majority of the components are printed in PLA (polylactic acid) plastic, thanks to its higher rigidity with respect to ABS (acrylonitrile–butadiene–styrene) or PETG (Polyethylene terephthalate glycol), with FDM technology, while the probe (centering cone) and the drogue are 3D printed in resin using a SLA (stereolithography) machine.
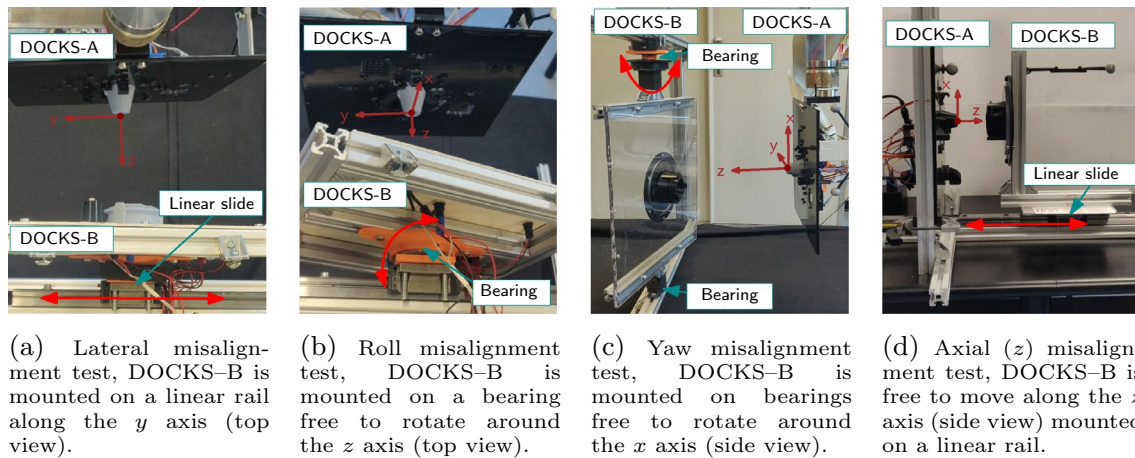
(a) Lateral misalignment test, DOCKS–B is mounted on a linear rail along the y axis (top view).

(b) Roll misalignment test, DOCKS–B is mounted on a bearing free to rotate around the z axis (top view).

(c) Yaw misalignment test, DOCKS–B is mounted on bearings free to rotate around the x axis (side view).

(d) Axial (z) misalignment test, DOCKS–B is free to move along the z axis (side view) mounted on a linear rail.

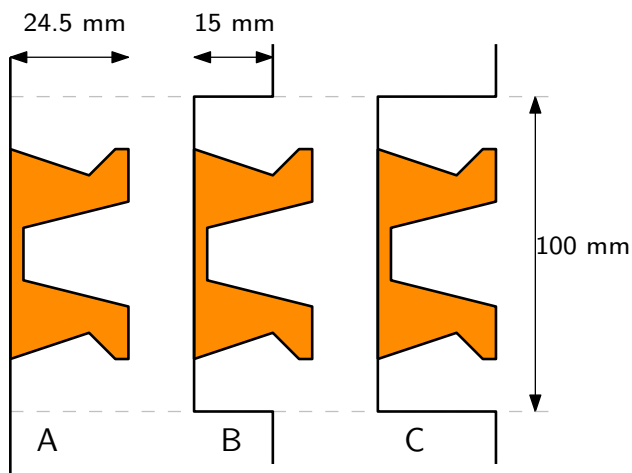Fig. 10 DOCKS mounting setup for the misalignment test

Fig. 11 Mounting configuration of the Drogue with respect to the MPCD plate

6.2 Test procedure

In this section, the procedure followed for the misalignment tolerance test is described. In particular, these tests are performed to evaluate the capabilities of the system to manage misalignments along the y axis, around the z axis (roll), around the x axis (yaw), and along the z axis. The first three tests follow a similar procedure. DOCKS–A is rigidly mounted on the end-effector of the robotic arm and DOCKS–B is mounted in a neutral position on the dedicated supports, which vary with the type of test. The initial alignment of DOCKS–A and DOCKS–B is carried out without imposing a misalignment in order to set the "zero" position of the robotic arm and calibrate the motion capture system. After the first alignment, the tests proceed as follows:

1. DOCKS-A is positioned 50mm away from the "zero" position;
2. A small misalignment is imposed on DOCKS-B, and measured by the motion capture system;
3. The robotic arm drives DOCKS–A following a straight trajectory towards DOCKS–B with a linear velocity of 1cm/s;
4. Once the two parts are aligned, the fork sensors provide the acknowledgement signal and the claws are activated.
5. If the test run has been successful, it is repeated increasing the misalignment by a fixed step. If the test has failed, it is repeated lowering the misalignment by half the fixed step. In case of success, the current misalignment value is set to be the maximum acceptable, in case of failure the final acceptable value is set to be the one of the last successful test.

When testing the misalignment along yaw, the docking procedure is considered failed if a collision occurs between the holding structures of DOCKS–A and DOCKS–B, regardless if hard–docking is achieved.

For the last test, along the z axis, the robotic arm is not used. A misalignment is set between the DOCKS–A and DOCKS–B and the claws are actuated. If the claws are able to capture the drogue, the test is successful. The misalignment increase/decrease follows the same logic as for the other tests.

6.3 Results

For each test, multiple runs have been executed to validate the repeatability. The misalignment values have been extrapolated through the post-processing of the motion capture data. The results, as numerical values, are summarized in Table 4, where the minimum misalignment value tested, the

step size used and the maximum acceptable misalignment value are shown. Figure 12 shows the results, in terms of plots, of one of the test performed for each of the four cases.

Figure 12a shows the behaviour of the system during the lateral misalignment test, along the *y* axis. In the lower part of the figure, it is noticeable that the two parts do not align around 0 but around the 3mm value. This behaviour is related to two factors: the first one is the non-ideal behaviour of the linear rails due to the presence of some friction; the second can be identified in the backlash of the robotic arm. Both of these issues do not invalidate the results presented. In fact, the relative position of DOCKS–A and DOCKS–B, represented by the dotted line in the figure, shows the desired behaviour. Figure 12b shows the behaviour of the system during the roll misalignment test (around the *z* axis), and Fig. 12c represents the yaw misalignment test (around the *x* axis) in configuration A. Configurations B and C have a similar behaviour, but they are able to manage lower misalignment. In Fig. 12d the result of the misalignment test along the *z* axis visible. In all of the aforementioned figures, the dotted line represents the relative motion between the two parts of the system. In all figures, the final relative misalignment is zero. As shown in [3], a combination of angular and linear misalignments tend to shift the range of acceptability but not its amplitude. Depending on the misalignment combination, the maximum acceptable value for each of them lowers.

Table 4 Results of misalignment tests

Lateral misalignment (along **y**)	Value
Step size [mm]	1
Minimum tested value [mm]	3
Maximum acceptable value [mm]	9
Roll misalignment (around **z**)	Value
Step size [deg]	1
Minimum tested value [deg]	2
Maximum acceptable value [deg]	8.5
Yaw misalignment (around **x**)	Value
Step size [deg]	1
Minimum value tested [deg]	2
A) Maximum acceptable value [deg]	9
B) Maximum acceptable value [deg]	6.5
C) Maximum acceptable value [deg]	3
Axial misalignment (along **z**)	Value
Step size [mm]	0.5
Minimum value tested [mm]	1
Maximum acceptable value [mm]	2.5

7 Load tests

The load test on the system was performed under different conditions to thoroughly evaluate the behaviour of the system. The maximum load that the laboratory prototype is capable of handling is determined under three conditions:

1. *Soft docking*: EM active, claws open.
2. *Hard docking (active)*: EM inactive, claws closed and active.
3. *Hard docking (passive)*: EM inactive, claws closed and not actuated.

A dead mass of known weight is added to DOCKS–B before connecting it to DOCKS–A, each test is considered successful if the two parts remain connected for at least 10s. The waiting time is set to be enough to ensure that the system has reached a steady state. The success criteria, in terms of load, is set, as a mission requirement, to be 10N during soft docking and 20N during hard docking with the claws active.

Soft docking. The load test on the soft docking is conducted connecting DOCKS–A and DOCKS–B only through the EM active. To test the capabilities of the EM, an additional dead mass is added to DOCKS–A to reach a total mass of 1.05kg, equivalent to 10.3N. The test is repeated 10 times with a success rate of 100%.

Hard docking (active). These tests aim to verify the ability of DOCKS–A to hold a load with three and two actuated claws, respectively. The load is applied to DOCKS–B. Each test is repeated three times. With three claws active, the system is able to lift and hold a mass of 3.0kg, equivalent to 29.4N. While with only two active claws and the third in the open position, the maximum load lowers to 19.6N (2.0kg).

Hard docking (passive). For these tests, all claws are in a closed configuration around the drogue, but the servomotors are not powered. The load is sustained only by the geometry of the system. The test succeeded at a maximum load of 10.3N (1.05kg).

8 Conclusions

This paper discusses the mechanical design and testing of a docking system for CubeSat called DOCKS. The work is conducted in the framework of the Space Rider Observer Cube (SROC) mission. SROC is a CubeSat designed to be deployed by Space Rider, to execute inspection operations on SR and to finally dock back to the mothership before re-entering the Earth atmosphere. DOCKS is a smart integrated docking system. This solution is standalone and is composed of a mechanical interface, a suite of sensors and a dedicated computer. The mechanical interface is based on
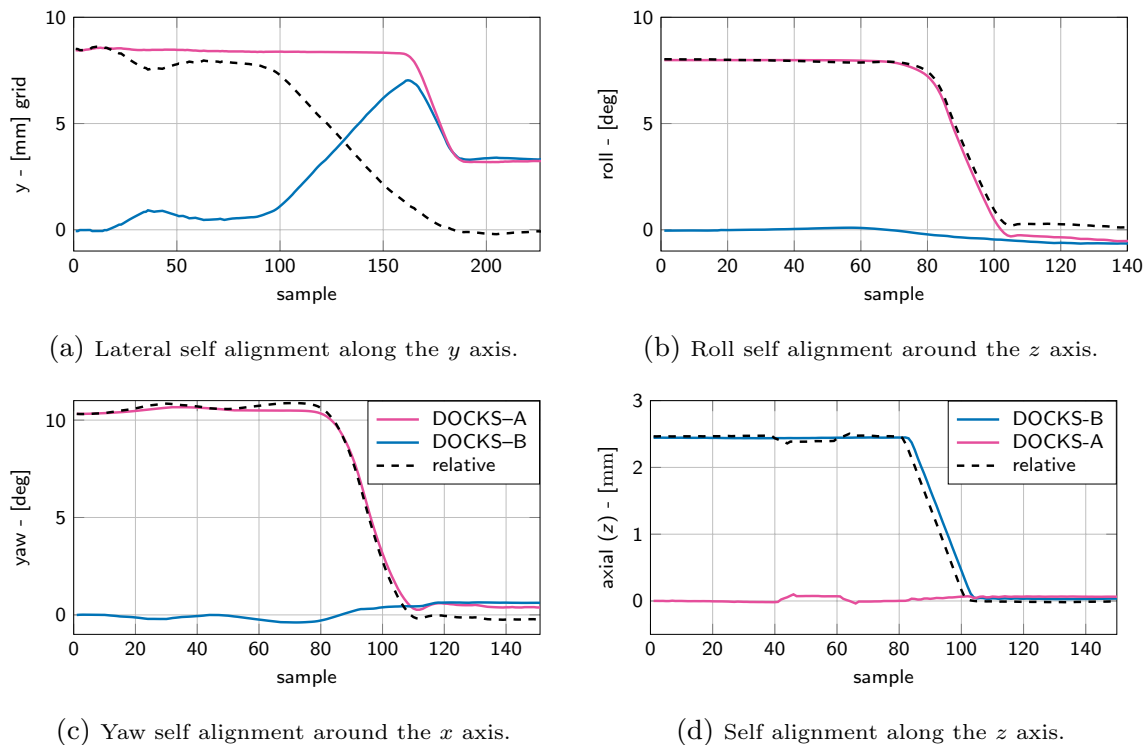
(a) Lateral self alignment along the y axis.

(b) Roll self alignment around the z axis.

(c) Yaw self alignment around the x axis.

(d) Self alignment along the z axis.

Fig. 12 Results of the maximum misalignment of the self alignment tests. The dashed line represents the relative motion between DOCKS–A and DOCKS–B

a probe–drogue design with the addition of a gripper-like interface to ensure the connection. After a brief overview of the docking system, the paper presents the validation tests conducted on the mechanical interface to prove its ability to manage misalignment. The results show that the system is compliance with the mission requirements. In fact, the system is able to manage misalignment up to 9mm along the y axis, 8.5deg on roll (around the z axis), 9deg on yaw (around the x axis) depending on the configuration and 2.5mm along the z axis.

Declarations

Conflict of interest The authors declare that they have no known competing financial interests or personal relationships that could have appeared to influence the work reported in this paper.

References

1. Corpino, S., Ammirante, G., Daddi, G., Stesina, F., Corradino, F., Basler, A., Francesconi, A., Branz, F., Van den Eynde, J.: Space rider observer cube - sroc: a cubesat mission for proximity operations demonstration. In: 73rd International Astronautical Congress (2022)

2. Cook, J., Aksamentov, V., Hoffman, T., Bruner, W.: Iss interface mechanisms and their heritage. In: AIAA SPACE 2011 Conference & Exposition, p. 7150 (2011)

3. Branz, F., Olivieri, L., Sansone, F., Francesconi, A.: Miniature docking mechanism for CubeSats. Acta Astronautica **176**, 510–519 (2020). https://doi.org/10.1016/j.actaastro.2020.06.042

4. Boesso, A., Francesconi, A.: ARCADE small-scale docking mechanism for micro-satellites. Acta Astronautica **86**, 77–87 (2013). https://doi.org/10.1016/j.actaastro.2013.01.006

5. Barbetta, M., Boesso, A., Branz, F., Carron, A., Olivieri, L., Prendin, J., Rodeghiero, G., Sansone, F., Savioli, L., Spinello, F., Francesconi, A.: ARCADE-R2 experiment on board BEXUS 17 stratospheric balloon. CEAS Space J **7**(3), 347–358 (2015). https://doi.org/10.1007/s12567-015-0083-3

6. Mohan, S., Saenz-Otero, A., Nolet, S., Miller, D.W., Sell, S.: SPHERES flight operations testing and execution. Acta Astronautica **65**(7–8), 1121–1132 (2009). https://doi.org/10.1016/j.actaastro.2009.03.039

7. Olivieri, L., Francesconi, A.: Design and test of a semiandrogynous docking mechanism for small satellites. Acta Astronautica **122**, 219–230 (2016). https://doi.org/10.1016/j.actaastro.2016.02.004

8. Underwood, C., Pellegrino, S., Lappas, V.J., Bridges, C.P., Baker, J.: Using CubeSat/micro-satellite technology to demonstrate the autonomous assembly of a reconfigurable space telescope (AAReST). Acta Astronautica **114**, 112–122 (2015). https://doi.org/10.1016/j.actaastro.2015.04.008

9. Letier, P., Siedel, T., Deremetz, M., Pavlovskis, E., Lietaer, B., Nottensteiner, K., Roa Garzon, M.A., Sánchez Garcia, J., Corella, J.L., Gancet, J.: Hotdock: Design and validation of a new generation of standard robotic interface for on-orbit servicing. In: 71st International Astronautical Congress (2020)

10. Roscoe, C.W.T., Westphal, J.J., Mosleh, E.: Overview and GNC design of the CubeSat proximity operations demonstration (CPOD) mission. Acta Astronautica **153**, 410–421 (2018). https://doi.org/10.1016/j.actaastro.2018.03.033

11. Pirat, C.S., Mäusli, P.-A., Walker, R., Ankersen, F., Gass, V.: Guidance, navigation and control for autonomous cooperative docking of cubesats. In: The 4S Symposium 2018 (2018)

12. Samadikhoshkho, Z., Zareinia, K., Janabi-Sharifi, F.: A brief review on robotic grippers classifications. In: 2019 IEEE Canadian Conference of Electrical and Computer Engineering (CCECE), pp. 1–4 (2019). IEEE

13. Sansone, F., Branz, F., Francesconi, A.: A relative navigation sensor for CubeSats based on LED fiducial markers. Acta Astronautica **146**, 206–215 (2018). https://doi.org/10.1016/j.actaastro.2018.02.028

14. Caon, A., Peruffo, M., Branz, F., Francesconi, A.: Consensus sensor fusion to estimate the relative attitude during space capture operations. In: 2022 IEEE 9th International Workshop on Metrology for AeroSpace (MetroAeroSpace), pp. 299–304 (2022). IEEE

15. Caon, A., Branz, F., Francesconi, A.: Characterization of a new positioning sensor for space capture. In: 2021 IEEE 8th International Workshop on Metrology for AeroSpace (MetroAeroSpace), pp. 424–429 (2021). IEEE

16. Seelig, F.: Flexural pivots for space applications. In: JPL PROC. of the 3RD Aerospace Mech. Symp (1968)

17. Caon, A., Branz, F., Francesconi, A.: Development and test of a robotic arm for experiments on close proximity operations. Acta Astronautica **195**, 287–294 (2022). https://doi.org/10.1016/j.actaastro.2022.03.006